Dynamics of perturbations around inhomogeneous backgrounds in the HMF model

J. Stat. Mech. (2010) P08002

(http://iopscience.iop.org/1742-5468/2010/08/P08002)

Journal of Statistical Mechanics: Theory and Experiment
An IOP and SISSA journal

Dynamics of perturbations around inhomogeneous backgrounds in the HMF model

Julien Barré[1], **Alain Olivetti**[1] **and Yoshiyuki Y Yamaguchi**[2]

[1] Laboratoire J.A. Dieudonné, Université de Nice Sophia-Antipolis, UMR CNRS 6621, Parc Valrose, F-06108 Nice Cedex 02, France
[2] Department of Applied Mathematics and Physics, Graduate School of Informatics, Kyoto University, Kyoto 606-8501, Japan
E-mail: jbarre@unice.fr, alain.olivetti@unice.fr and yyama@amp.i.kyoto-u.ac.jp

Received 15 March 2010
Accepted 30 June 2010
Published 3 August 2010

Online at stacks.iop.org/JSTAT/2010/P08002
doi:10.1088/1742-5468/2010/08/P08002

Abstract. We investigate the dynamics of perturbations around inhomogeneous stationary states of the Vlasov equation corresponding to the Hamiltonian mean-field model. The inhomogeneous background induces a separatrix in the one-particle Hamiltonian system, and branch cuts generically appear in the analytic continuation of the dispersion relation in the complex frequency plane. We test the theory by direct comparisons with N-body simulations, using two families of distributions: inhomogeneous water-bags, and inhomogeneous thermal equilibria. In the water-bag case, which is not generic, no branch cut appears in the dispersion relation, whereas in the thermal equilibrium case, when looking for the root of the dispersion relation closest to the real axis, we have to consider several Riemann sheets. In both cases, we show that the roots of the continued dispersion relation give information that is useful for understanding the dynamics of a perturbation, although it is not complete.

Keywords: kinetic theory of gases and liquids

J. Stat. Mech. (2010) P08002

Contents

1. Introduction

The dynamical behavior and the relaxation to equilibrium of long-range interacting systems of particles still offer several open problems. It is possible to sketch the general theory as follows. The short time behavior, on the order of the dynamical timescale, is described by the Vlasov, or a Vlasov-like equation [1, 2]. The system then settles into a quasi-stationary state (hereafter called QSS), which is a stationary solution of the Vlasov equation. On timescales diverging with the number of particles, the system evolves towards the thermodynamic equilibrium, following the analog of a Lenard–Balescu equation (for a recent review, see [3]). The open questions include for instance the selection of the QSS among the stationary states of the Vlasov equation; the possible selection of periodic solutions of the Vlasov equation instead of a QSS; the complete understanding of the timescales for relaxation to equilibrium, especially around inhomogeneous QSS and close to dynamical transitions. We may mention also the rigorous derivation of the Lenard–Balescu equation, which, in contrast to the Vlasov equation, does not have a mathematical foundation.

The stationary solutions of the Vlasov equation are homogeneous or inhomogeneous in space. The former case is often studied in plasma physics, and the latter is the rule in self-gravitating systems. In general, there is less understanding of the inhomogeneous

J. Stat. Mech. (2010) P08002

cases, even at the level of linear perturbations of the Vlasov stationary state, because of the much greater technical difficulties; see [4] for a recent preprint on the kinetic theory of the inhomogeneous systems. This linear understanding is an essential ingredient for deriving a Lenard–Balescu-like equation, (see [5] for a textbook reference in the plasma physics context; see [6] for computations around inhomogeneous stationary states) and also for characterizing possible undamped periodic solutions [7, 8].

The linearization around a homogeneous stationary state corresponds to the usual theory of Landau damping in plasma physics [9]. Technically, the equations are solved by using a Fourier transform in space and a Laplace transform in time. The equations for different Fourier modes decouple, and the computation results in the complex dielectric function $\epsilon(k, \omega)$ for the kth Fourier mode. Because $\epsilon(k, \omega)$ is defined in the upper half of the ω-plane due to the convergence condition of the Laplace transform, one needs to analytically continue $\epsilon(k, \omega)$ in the lower half of the ω-plane to obtain the Landau frequency and damping rate.

Linearization around an inhomogeneous stationary state brings about additional technical difficulties. First, one needs to use angle–action variables, to simplify the particle dynamics; but now the equations for different Fourier modes in the angle variables do not decouple any longer; the analog of the dielectric function is now the determinant of an infinite matrix. We will from now on call this determinant a 'dispersion function'; its roots yield the eigenmodes and Landau poles of the linearized equation under study. Linearization around inhomogeneous stationary states has been studied in the context of self-gravitating systems, and, despite the technical difficulties, the above procedure has been carried out entirely to study the instability of some galactic models [10]–[15] (this list is far from being exhaustive). We also mention here some studies devoted to the investigation of purely oscillatory modes in a one-dimensional self-gravitating system [16]–[18], since this system is closer to the toy model that we will use in this article.

However, studying the analog of Landau damping requires the analytic continuation part, and this is, in the words of Weinberg [14], a 'daunting task'. This difficulty was bypassed in [14, 19] by fitting $\epsilon(\omega)$ in the upper half of the ω-plane with rational functions. These are the only articles that we are aware of where there is a quantitative study of gravitational Landau damping, with an explicit derivation of damping rates and frequencies; see however [20] for a discussion of Landau damping in the gravitational context. This may seem surprising, but the explanation probably lies in the dissuasive complexity of such computations.

There has been much more work on the linearization of the 2D Euler equation (or similar equations) around vortices or shear flows, in the context of 2D fluid dynamics or of magnetically confined non-neutral plasmas. The 2D Euler equation is a close parent of the Vlasov equation, but it has no kinetic variable. These works were in particular motivated by the understanding of the so-called diocotron instability of vortices, by the study of weakly damped 'quasimodes', and the asymptotic algebraic decay of perturbations; see for instance [21]–[30]; this list is definitely not exhaustive. Technically, in this case, different angular Fourier modes decouple, but the resulting radial equations are not exactly solvable, except in exceptional cases [22]. It has been recognized in this context that the dispersion function presents branch points, to which are attached branch cuts; these branch points are associated with the local maxima and minima of the rotation frequency $\Omega(r)$ (which plays the same role as the frequency as a function of the action

J. Stat. Mech. (2010) P08002

$\Omega(J)$ in the Vlasov case), including the boundary points. These branch points make the analytical continuation procedure tricky (see for instance [27]), and are related to an algebraic asymptotic behavior of perturbations. We note that these branch points and branch cuts have, to our knowledge, not been seen in the self-gravitating case. It is possible that the studies of [14, 19] stayed far enough from the branch points that their influence was negligible.

In this paper, we study the linearization around inhomogeneous stationary states of a Vlasov equation, and study the analytical continuation of the dispersion function. We are interested in a case where $\Omega(J)$ is not monotonic, and presents a singularity due to a separatrix. Since we will use the 1D HMF model [31]–[33], which is a much simpler setting than a 3D self-gravitating system, we will be able to perform the analysis in more detail than in [14]; in particular, we will analytically continue the frequency $\Omega(J)$, and show the branch points and branch cuts of the dispersion function $\epsilon(\omega)$. Our findings are confronted with direct N-body numerical simulations.

2. Derivation of the 'dispersion relation' for a 1D Vlasov equation

For the sake of simplicity, we will use the attractive HMF model. It describes the motion of N particles on a ring, interacting through a cosine potential. The position of particle i is given by $\theta_i \in (-\pi, \pi]$; its conjugate momentum is p_i. The Hamiltonian is

$$H = \frac{1}{2}\sum_{i=1}^{N} p_i^2 - \frac{1}{2N}\sum_{i\neq j}\cos(\theta_i - \theta_j). \tag{1}$$

It can be seen as a model retaining only the first harmonic of the 1D gravitational interaction. Despite the simplicity of the model, which is due to its 1D character and the smoothness of the interaction, this model retains many qualitative properties of more realistic long-range interacting systems. Because of this feature, it has been widely used in the last decade as a toy model to investigate various statistical and dynamical properties of long-range interactions [3].

The corresponding Vlasov equation for the one-particle distribution $f(\theta, p, t)$ is

$$\frac{\partial f}{\partial t} + p\frac{\partial f}{\partial \theta} - \frac{\partial \phi[f]}{\partial \theta}\frac{\partial f}{\partial p} = 0, \tag{2}$$

where $\phi[f](\theta, t)$ is the self-consistent potential

$$\phi[f](\theta, t) = -\int_{-\infty}^{\infty} \mathrm{d}p' \int_{-\pi}^{\pi} \mathrm{d}\theta' \, \cos(\theta - \theta') f(\theta', p', t). \tag{3}$$

It is useful in the following to consider the magnetization

$$\mathbf{M} = M\mathrm{e}^{\mathrm{i}\psi} = M_x + \mathrm{i}M_y = \int_{-\infty}^{\infty} \mathrm{d}p \int_{-\pi}^{\pi} \mathrm{d}\theta \, f(\theta, p, t)\mathrm{e}^{\mathrm{i}\theta}, \tag{4}$$

and the potential is written as

$$\phi[f](\theta, t) = -M\cos(\theta - \psi). \tag{5}$$

If f is homogeneous in space, that is f only depends on the p variable, then the self-consistent potential vanishes: $M = 0$. Without loss of generality, we will choose in the

J. Stat. Mech. (2010) P08002

following $\psi = 0$, so that the minimum of the self-consistent potential in the stationary state will be located in $\theta = 0$.

The Vlasov equation is rewritten as

$$\partial_t f + [f, h] = 0, \tag{6}$$

where $[u, v]$ is the Poisson bracket between u and v, defined as

$$[u, v] = \frac{\partial u}{\partial \theta}\frac{\partial v}{\partial p} - \frac{\partial u}{\partial p}\frac{\partial v}{\partial \theta} \tag{7}$$

and

$$h[f](\theta, p, t) = \frac{p^2}{2} + \phi[f](\theta, t) = \frac{p^2}{2} - M\cos\theta. \tag{8}$$

Let f_0 depend on (θ, p) only through $h[f_0]$; then $f_0(h[f_0](\theta, p))$ is a stationary solution of the Vlasov equation (6). In the homogeneous case, any function of the energy $p^2/2$ is a stationary solution; in the inhomogeneous case, a self-consistent equation for $\phi[f_0]$, or equivalently for the magnetization M_0, needs to be satisfied, where M_0 denotes the modulus of the magnetization of f_0.

We study a perturbation f_1 around such a stationary solution f_0. The function f is hence expanded as

$$f = f_0 + f_1.$$

Substituting this expansion into the Vlasov equation (6) and neglecting higher order terms, f_1 satisfies the linearized Vlasov equation

$$\partial_t f + [f_1, h_0] + [f_0, h_1] = 0, \tag{9}$$

where

$$h_0(\theta, p) = \frac{p^2}{2} + \phi[f_0](\theta) = \frac{p^2}{2} - M_0\cos\theta \tag{10}$$

and

$$h_1(\theta, p, t) = \phi[f_1](\theta, t).$$

We define $\phi_1(\theta, t) = \phi[f_1](\theta, t)$. Note that f_0 is stationary and hence we omitted the argument t of h_0 and of $\phi[f_0]$.

We derive the dispersion relation from the linearized Vlasov equation (9). The first step is to use angle–action variables (w, J) instead of (θ, p) for the dynamics defined by the one-particle Hamiltonian (10). The angle–action variables are defined by using Legendre elliptic integrals. The elliptic integrals and the angle–action variables are introduced in appendices A and B respectively.

The action variable is defined by the area surrounded by a closed orbit; see (B.2). If the energy h_0 of the closed orbit is slightly smaller than the separatrix energy, which is M_0, then the orbit surrounds the shaded region of figure 1. On the other hand, if the energy is slightly larger than that of the separatrix, then the orbit only surrounds the upper (or lower) half of the shaded region. The area, and the value of action, is then divided by two. Because of this gap and of the symmetry between the upper and lower sides of the separatrix, the angle–action variables take the same values at three points shown in figure 1. The transformation $(\theta, p) \mapsto (w, J)$ is hence not injective.

J. Stat. Mech. (2010) P08002

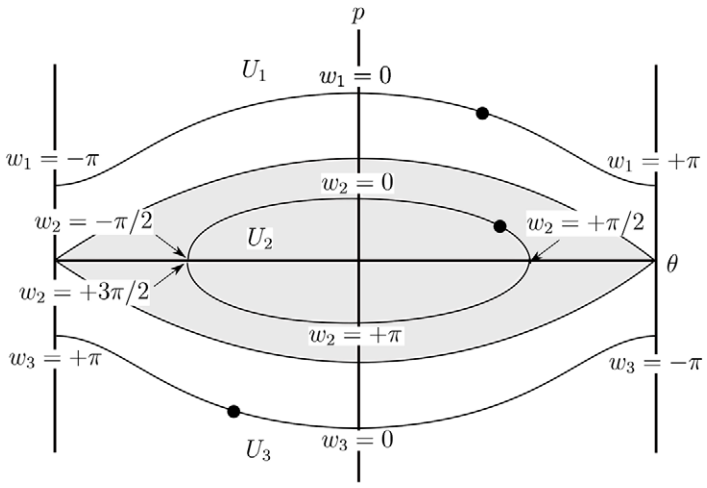

Figure 1. μ space for the one-particle Hamiltonian system $h_0(\theta, p)$ (10). The three black points have the same values of angle–action variables, and hence we divide μ space into three parts: U_1, U_2 and U_3. The shaded region is U_2. Values of the angle variable w_α are reported for three orbits in the three domains.

To construct bijective transformations, we divide μ space into the following three parts, where we name as μ space the (θ, p) domain $\mu = (-\pi, \pi] \times \mathbb{R}$:

$$\begin{aligned} U_1 &= \{(\theta, p) | h_0(\theta, p) > M_0, p > 0\}, \\ U_2 &= \{(\theta, p) | -M_0 < h_0(\theta, p) < M_0\}, \\ U_3 &= \{(\theta, p) | h_0(\theta, p) > M_0, p < 0\}. \end{aligned} \tag{11}$$

The domains U_1 and U_3 are outside of the separatrix and U_2 is inside. Thanks to the division of μ space, we can construct a bijective transformation on each of the U_α as

$$\varphi_\alpha : U_\alpha \to V_\alpha; \qquad (\theta, p) \mapsto (w_\alpha, J_\alpha),$$

and there exist inverse transformations $\varphi_\alpha^{-1} : V_\alpha \to U_\alpha$. For explicit expressions for V_α, w_α and J_α as functions of M_0 and of the old variables θ and p, see appendix B. Notice that the change of variables depends on the potential in the stationary state $\phi[f_0]$.

To obtain the dispersion relation, we need to compute integrals over μ space. Such an integral is written in the angle–action variables as follows: for a function f on μ space, the integral is divided into the three parts according to the division of μ space as

$$\int\int_\mu f(\theta, p)\, \mathrm{d}\theta\, \mathrm{d}p = \sum_{\alpha=1}^{3} \int\int_{U_\alpha} f(\theta, p)\, \mathrm{d}\theta\, \mathrm{d}p. \tag{12}$$

In the domain U_α, we can define the pull-back f_α of f with respect to the inverse transformation φ_α^{-1} by

$$f_\alpha(w_\alpha, J_\alpha) = f(\varphi_\alpha^{-1}(w_\alpha, J_\alpha)), \qquad (w_\alpha, J_\alpha) \in V_\alpha. \tag{13}$$

We remark that we can define the function f_α thanks to the existence of φ_α^{-1}, and to the division of μ space accordingly. The integral over μ space is then written in the

angle–action variables as

$$\int\int_{\mu} f(\theta,p)\,\mathrm{d}\theta\,\mathrm{d}p = \sum_{\alpha=1}^{3}\int\int_{V_\alpha} f_\alpha(w_\alpha,J_\alpha)\,\mathrm{d}w_\alpha\,\mathrm{d}J_\alpha, \tag{14}$$

since the transformations φ_α are canonical and $\mathrm{d}\theta\wedge\mathrm{d}p=\mathrm{d}w_\alpha\wedge\mathrm{d}J_\alpha$ holds.

We remark that the three domains U_α do not cover the whole μ-space, since

$$\mu = \bigcup_{\alpha=1}^{3} U_\alpha \bigcup\{(0,0)\}\bigcup\{\text{separatrix}\}. \tag{15}$$

However, this will not create any difficulty in the derivation of the dispersion relation, because what we need are integrals over μ, and the difference between μ and $\bigcup_\alpha U_\alpha$ is of zero measure.

The Vlasov equation (6), and the linearized Vlasov equation (9), are invariant under the canonical transformations φ_α, and the latter is written in V_α as

$$\partial_t f_{1,\alpha} + [f_{1,\alpha}, h_{0,\alpha}]_\alpha + [f_{0,\alpha}, h_{1,\alpha}]_\alpha = 0, \tag{16}$$

where the Poisson bracket is now written in terms of the new variables

$$[u_\alpha, v_\alpha]_\alpha = \frac{\partial u_\alpha}{\partial w_\alpha}\frac{\partial v_\alpha}{\partial J_\alpha} - \frac{\partial u_\alpha}{\partial J_\alpha}\frac{\partial v_\alpha}{\partial w_\alpha}. \tag{17}$$

Using the facts that $h_{0,\alpha}$ and $f_{0,\alpha}$ depend only on J_α, and defining the rotation frequency

$$\Omega_\alpha(J_\alpha) = \frac{\mathrm{d}h_{0,\alpha}}{\mathrm{d}J_\alpha}(J_\alpha), \tag{18}$$

the linearized Vlasov equation (16) becomes

$$\frac{\partial f_{1,\alpha}}{\partial t} + \Omega_\alpha\frac{\partial f_{1,\alpha}}{\partial w_\alpha} - \frac{\mathrm{d}f_{0,\alpha}}{\mathrm{d}J_\alpha}\frac{\partial \phi_{1,\alpha}}{\partial w_\alpha} = 0. \tag{19}$$

The rotation frequencies Ω_α are plotted in figure 2. Ω_2 takes its maximum value at the bottom of the potential well $J_2=0$, and decreases to 0 with a singularity at the separatrix (see equation (B.9)). $\Omega_1=\Omega_3$, and they increase from 0 at the separatrix, where they are also singular, to $+\infty$ (see equation (B.9)). In the large J limit, the potential well is negligible and the $\Omega_\alpha(J_\alpha)$ relation is almost linear.

To derive the dispersion relation from (19), we define the Fourier–Laplace transform $\hat{u}(m,J,\omega)$ of a function $u(w,J,t)$ as

$$\hat{u}(m,J,\omega) = \int_{-\pi}^{\pi}\mathrm{d}w\,\mathrm{e}^{-\mathrm{i}mw}\int_{0}^{+\infty}\mathrm{d}t\,\mathrm{e}^{\mathrm{i}\omega t}u(w,J,t) \tag{20}$$

where m is an integer and $\mathrm{Im}(\omega)$ large enough to ensure convergence. The integration interval with respect to w must be shifted to $(-\pi/2,3\pi/2]$ in V_2. The inverse transform is then

$$u(w,J,t) = \frac{1}{(2\pi)^2}\sum_{m=-\infty}^{\infty}\int_{\Gamma}\mathrm{d}\omega\,\hat{u}(m,J,\omega)\mathrm{e}^{-\mathrm{i}\omega t}\,\mathrm{e}^{\mathrm{i}mw} \tag{21}$$

where Γ is a Bromwich contour running from $-\infty+\mathrm{i}\sigma$ to $+\infty+\mathrm{i}\sigma$, and the real value σ is larger than the imaginary part of any singularity of $\hat{u}(m,J,\omega)$ in the complex ω-plane.

J. Stat. Mech. (2010) P08002

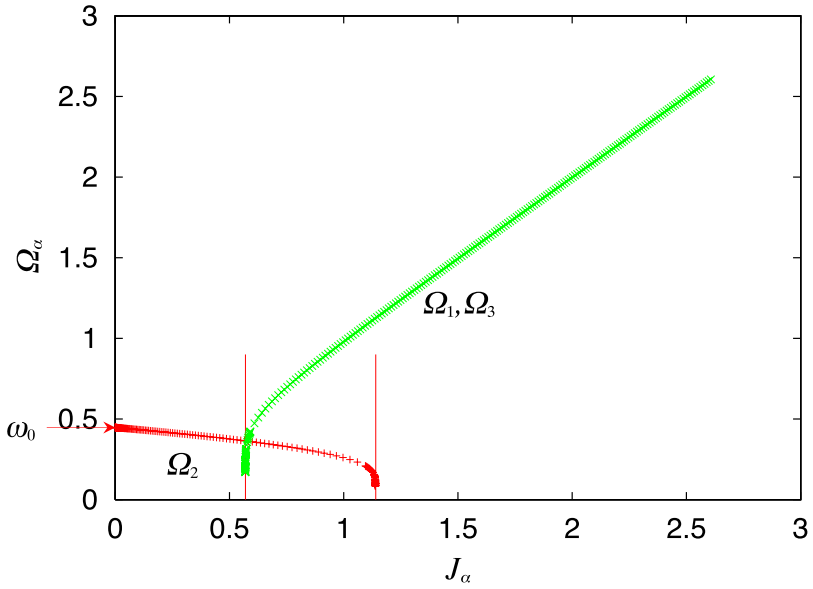

Figure 2. Frequencies Ω_α as functions of J_α for $M_0 = 0.2$, and $\omega_0 = \lim_{J_2 \to 0} \Omega_2(J_2) = \sqrt{M_0} = 0.447\ldots$ accordingly. The two vertical lines mark the values of actions corresponding to the separatrix, which are $J_1 = J_3 = 4\omega_0/\pi$ and $J_2 = 8\omega_0/\pi$.

We perform a Fourier–Laplace transform on equation (19). This yields, after simple algebraic manipulations,

$$\hat{f}_{1,\alpha}(m, J_\alpha, \omega) = \frac{m f'_{0,\alpha}(J_\alpha)}{m\Omega_\alpha(J_\alpha) - \omega} \hat{\phi}_{1,\alpha}(m, J_\alpha, \omega) + \frac{g_\alpha(m, J_\alpha)}{m\Omega_\alpha(J_\alpha) - \omega} \tag{22}$$

where $g_\alpha(m, J_\alpha) = -\mathrm{i} f^F_{1,\alpha}(m, J_\alpha, 0)$ and $f^F_{1,\alpha}(m, J_\alpha, 0)$ is the Fourier transform with respect to w_α of $f_{1,\alpha}(w_\alpha, J_\alpha, 0)$, the initial value of the perturbation.

We need to introduce this last equation (22) into the definition of the perturbation potential $\phi_{1,\alpha}$ for self-consistency. This task is complicated by the fact that $f_{1,\alpha}$ is naturally expanded in a Fourier series in the angle variable w_α, whereas $\phi_{1,\alpha}$ is naturally expanded in a Fourier series in the original spatial variable θ. As a consequence, the equations for different Fourier modes do not decouple, at variance with what happens in the usual homogeneous case. Then, for the perturbation potential, we have

$$\begin{aligned}
\hat{\phi}_{1,\alpha}(m, J_\alpha, \omega) = \int_{-\pi}^{\pi} \mathrm{d}w_\alpha \, \mathrm{e}^{-\mathrm{i}m w_\alpha} \int_0^{+\infty} \mathrm{d}t \, \mathrm{e}^{\mathrm{i}\omega t} \phi_{1,\alpha}(\theta_\alpha, t) = -\int_{-\pi}^{\pi} \mathrm{d}w_\alpha \cos\theta_\alpha \mathrm{e}^{-\mathrm{i}m w_\alpha} \\
\times \frac{1}{2\pi} \sum_{m'} \sum_{\alpha'} \int \int_{V_{\alpha'}} \cos\theta'_{\alpha'} \mathrm{e}^{\mathrm{i}m' w'_{\alpha'}} \hat{f}_{1,\alpha'}(m', J'_{\alpha'}, \omega) \, \mathrm{d}w'_{\alpha'} \, \mathrm{d}J'_{\alpha'} \\
- \int_{-\pi}^{\pi} \mathrm{d}w_\alpha \sin\theta_\alpha \mathrm{e}^{-\mathrm{i}m w_\alpha} \frac{1}{2\pi} \sum_{m'} \sum_{\alpha'} \int \int_{V_{\alpha'}} \sin\theta'_{\alpha'} \mathrm{e}^{\mathrm{i}m' w'_{\alpha'}} \hat{f}_{1,\alpha'}(m', J'_{\alpha'}, \omega) \\
\times \mathrm{d}w'_{\alpha'} \, \mathrm{d}J'_{\alpha'},
\end{aligned} \tag{23}$$

where θ_α is the first element of the mapping $\varphi_\alpha^{-1}(w_\alpha, J_\alpha) = (\theta_\alpha(w_\alpha, J_\alpha), J_\alpha(w_\alpha, J_\alpha))$. In the course of computations we have used the equality (14).

We define

$$c_{m,\alpha}(J_\alpha) = \int_{-\pi}^{\pi} \cos\theta_\alpha \mathrm{e}^{\mathrm{i}mw_\alpha}\,\mathrm{d}w_\alpha \qquad s_{m,\alpha}(J_\alpha) = \int_{-\pi}^{\pi} \sin\theta_\alpha \mathrm{e}^{\mathrm{i}mw_\alpha}\,\mathrm{d}w_\alpha \tag{24}$$

and

$$\begin{aligned}\Sigma_C(\omega) &= \frac{1}{2\pi}\sum_m\sum_\alpha \int\int_{V_\alpha} \cos\theta_\alpha \mathrm{e}^{\mathrm{i}mw_\alpha}\hat{f}_{1,\alpha}(m,J_\alpha,\omega)\,\mathrm{d}w_\alpha\,\mathrm{d}J_\alpha \\ \Sigma_S(\omega) &= \frac{1}{2\pi}\sum_m\sum_\alpha \int\int_{V_\alpha} \sin\theta_\alpha \mathrm{e}^{\mathrm{i}mw_\alpha}\hat{f}_{1,\alpha}(m,J_\alpha,\omega)\,\mathrm{d}w_\alpha\,\mathrm{d}J_\alpha.\end{aligned} \tag{25}$$

If we call $\mathbf{M}_1(t) = M_{1,x}(t) + \mathrm{i}M_{1,y}(t)$ the perturbation in magnetization, then $\Sigma_C(\omega)$ and $\Sigma_S(\omega)$ are nothing but the Laplace transforms of $M_{1,x}(t)$ and $M_{1,y}(t)$ respectively. The Fourier–Laplace component $\hat{\phi}_{1,\alpha}(m,J_\alpha,\omega)$ is written as

$$\hat{\phi}_{1,\alpha}(m,J_\alpha,\omega) = -[\bar{c}_{m,\alpha}(J_\alpha)\Sigma_C(\omega) + \bar{s}_{m,\alpha}(J_\alpha)\Sigma_S(\omega)] \tag{26}$$

where $\bar{c}_{m,\alpha}$ and $\bar{s}_{m,\alpha}$ are the complex conjugates of $c_{m,\alpha}$ and $s_{m,\alpha}$ respectively. Substituting $\hat{\phi}_{1,\alpha}(m,J_\alpha,\omega)$ into equation (22), $\hat{f}_{1,\alpha}(m,J_\alpha,\omega)$ is

$$\hat{f}_{1,\alpha}(m,J_\alpha,\omega) = \frac{-mf'_{0,\alpha}(J_\alpha)}{m\Omega_\alpha(J_\alpha)-\omega}[\bar{c}_{m,\alpha}(J_\alpha)\Sigma_C(\omega) + \bar{s}_{m,\alpha}(J_\alpha)\Sigma_S(\omega)] + \frac{g_\alpha(m,J_\alpha)}{m\Omega_\alpha(J_\alpha)-\omega}. \tag{27}$$

We now multiply equation (27) by $\cos\theta_\alpha \mathrm{e}^{\mathrm{i}mw_\alpha}$ or $\sin\theta_\alpha \mathrm{e}^{\mathrm{i}mw_\alpha}$, integrate over V_α, sum over α and m, and divide by 2π. This yields two equations:

$$\begin{aligned}\Sigma_C(\omega) = &-\frac{1}{2\pi}\sum_m\sum_\alpha \int\int_{V_\alpha} \frac{mf'_{0,\alpha}(J_\alpha)}{m\Omega_\alpha(J_\alpha)-\omega}\bar{c}_{m,\alpha}(J_\alpha)\cos\theta_\alpha \mathrm{e}^{\mathrm{i}mw_\alpha}\,\mathrm{d}w_\alpha\,\mathrm{d}J_\alpha\Sigma_C(\omega) \\ &- \frac{1}{2\pi}\sum_m\sum_\alpha \int\int_{V_\alpha} \frac{mf'_{0,\alpha}(J_\alpha)}{m\Omega_\alpha(J_\alpha)-\omega}\bar{s}_{m,\alpha}(J_\alpha)\cos\theta_\alpha \mathrm{e}^{\mathrm{i}mw_\alpha}\,\mathrm{d}w_\alpha\,\mathrm{d}J_\alpha\Sigma_S(\omega) \\ &+ \frac{1}{2\pi}\sum_m\sum_\alpha \int\int_{V_\alpha} \frac{g_\alpha(m,J_\alpha)}{m\Omega_\alpha(J_\alpha)-\omega}\cos\theta_\alpha \mathrm{e}^{\mathrm{i}mw_\alpha}\mathrm{d}w_\alpha\,\mathrm{d}J_\alpha \\ \Sigma_S(\omega) = &-\frac{1}{2\pi}\sum_m\sum_\alpha \int\int_{V_\alpha} \frac{mf'_{0,\alpha}(J_\alpha)}{m\Omega_\alpha(J_\alpha)-\omega}\bar{c}_{m,\alpha}(J_\alpha)\sin\theta_\alpha \mathrm{e}^{\mathrm{i}mw_\alpha}\,\mathrm{d}w_\alpha\,\mathrm{d}J_\alpha\Sigma_C(\omega) \\ &- \frac{1}{2\pi}\sum_m\sum_\alpha \int\int_{V_\alpha} \frac{mf'_{0,\alpha}(J_\alpha)}{m\Omega_\alpha(J_\alpha)-\omega}\bar{s}_{m,\alpha}(J_\alpha)\sin\theta_\alpha \mathrm{e}^{\mathrm{i}mw_\alpha}\,\mathrm{d}w_\alpha\,\mathrm{d}J_\alpha\Sigma_S(\omega) \\ &+ \frac{1}{2\pi}\sum_m\sum_\alpha \int\int_{V_\alpha} \frac{g_\alpha(m,J_\alpha)}{m\Omega_\alpha(J_\alpha)-\omega}\sin\theta_\alpha \mathrm{e}^{\mathrm{i}mw_\alpha}\mathrm{d}w_\alpha\,\mathrm{d}J_\alpha.\end{aligned} \tag{28}$$

J. Stat. Mech. (2010) P08002

To express the dispersion relation in a compact form, we introduce one more time some notation:

$$\begin{aligned}
F_{\bar{c}c}(\omega) &= \frac{1}{2\pi}\sum_m\sum_\alpha \int\!\!\int_{V_\alpha} \frac{m f'_{0,\alpha}(J_\alpha)}{m\Omega_\alpha(J_\alpha)-\omega}\bar{c}_{m,\alpha}(J_\alpha)\cos\theta_\alpha \mathrm{e}^{\mathrm{i}mw_\alpha}\,\mathrm{d}w_\alpha\,\mathrm{d}J_\alpha,\\
F_{\bar{s}c}(\omega) &= \frac{1}{2\pi}\sum_m\sum_\alpha \int\!\!\int_{V_\alpha} \frac{m f'_{0,\alpha}(J_\alpha)}{m\Omega_\alpha(J_\alpha)-\omega}\bar{s}_{m,\alpha}(J_\alpha)\cos\theta_\alpha \mathrm{e}^{\mathrm{i}mw_\alpha}\,\mathrm{d}w_\alpha\,\mathrm{d}J_\alpha,\\
F_{\bar{c}s}(\omega) &= \frac{1}{2\pi}\sum_m\sum_\alpha \int\!\!\int_{V_\alpha} \frac{m f'_{0,\alpha}(J_\alpha)}{m\Omega_\alpha(J_\alpha)-\omega}\bar{c}_{m,\alpha}(J_\alpha)\sin\theta_\alpha \mathrm{e}^{\mathrm{i}mw_\alpha}\,\mathrm{d}w_\alpha\,\mathrm{d}J_\alpha,\\
F_{\bar{s}s}(\omega) &= \frac{1}{2\pi}\sum_m\sum_\alpha \int\!\!\int_{V_\alpha} \frac{m f'_{0,\alpha}(J_\alpha)}{m\Omega_\alpha(J_\alpha)-\omega}\bar{s}_{m,\alpha}(J_\alpha)\sin\theta_\alpha \mathrm{e}^{\mathrm{i}mw_\alpha}\,\mathrm{d}w_\alpha\,\mathrm{d}J_\alpha,
\end{aligned} \tag{29}$$

and

$$\begin{aligned}
G_c(\omega) &= \frac{1}{2\pi}\sum_m\sum_\alpha \int\!\!\int_{V_\alpha} \frac{g_\alpha(m,J_\alpha)}{m\Omega_\alpha(J_\alpha)-\omega}\cos\theta_\alpha \mathrm{e}^{\mathrm{i}mw_\alpha}\,\mathrm{d}w_\alpha\,\mathrm{d}J_\alpha,\\
G_s(\omega) &= \frac{1}{2\pi}\sum_m\sum_\alpha \int\!\!\int_{V_\alpha} \frac{g_\alpha(m,J_\alpha)}{m\Omega_\alpha(J_\alpha)-\omega}\sin\theta_\alpha \mathrm{e}^{\mathrm{i}mw_\alpha}\,\mathrm{d}w_\alpha\,\mathrm{d}J_\alpha.
\end{aligned}$$

Using this notation, the two equations (28) are expressed in the following matrix form:

$$\begin{pmatrix} 1+F_{\bar{c}c}(\omega) & F_{\bar{s}c}(\omega) \\ F_{\bar{c}s}(\omega) & 1+F_{\bar{s}s}(\omega)\end{pmatrix}\begin{pmatrix}\Sigma_C(\omega)\\ \Sigma_S(\omega)\end{pmatrix} = \begin{pmatrix} G_c(\omega)\\ G_s(\omega)\end{pmatrix}. \tag{30}$$

This matrix equation is actually diagonal, as can be shown using the relations for the c_m and s_m functions (B.10) and (B.11); see appendix B. Indeed, in region V_2, the products $\bar{c}_m s_m$ and $\bar{s}_m c_m$ vanish thanks to (B.11); and the contributions to $F_{\bar{c}s}$ and $F_{\bar{s}c}$ coming from regions V_1 and V_3 cancel one another thanks to (B.10). Thus $F_{\bar{c}s}(\omega) = F_{\bar{s}c}(\omega) = 0$.

The dispersion relation is given by $\epsilon(\omega) = 0$, with the dispersion function

$$\epsilon(\omega) = [1+F_{\bar{c}c}(\omega)][1+F_{\bar{s}s}(\omega)]. \tag{31}$$

Hence the perturbation's potential is

$$\hat{\phi}_{1,\alpha}(m,J_\alpha,\omega) = -\frac{G_c(\omega)}{1+F_{\bar{c}c}(\omega)}\bar{c}_{m,\alpha}(J_\alpha) - \frac{G_s(\omega)}{1+F_{\bar{s}s}(\omega)}\bar{s}_{m,\alpha}(J_\alpha). \tag{32}$$

The time evolution of ϕ_1 is given by the inverse Fourier–Laplace transform of equation (32).

We have concentrated in this section on the HMF case for the sake of simplicity; see appendix C for some comments on the case of general potentials.

3. Analytic continuation

To solve the initial value problem for the perturbation f_1, or the perturbation potential ϕ_1, we need to perform the inverse Laplace transform (21) on $\hat{f}_1$, or Σ_C and Σ_S. For this purpose, it is useful to deform the Bromwich contour Γ, and to study the singularities of the integrand, or rather of its analytic continuation, in the complex ω-plane. From equation (32), we see that these singularities may come from singularities in the $F_{\bar{c}c}$, $F_{\bar{s}s}$, G_c or G_s, or from roots of $\epsilon(\omega)$. From the analogy with Landau damping around

J. Stat. Mech. (2010) P08002

homogeneous stationary states, one would expect these roots of $\epsilon(\omega)$ to give damped and oscillating contributions to the time evolution of perturbations, when the reference state is stable. However, other singularities of $\epsilon(\omega)$ may contribute to this time evolution; thus in the following, we will also investigate the singularities of $\epsilon(\omega)$.

The Fourier–Laplace transformation $\hat{f}_{1,\alpha}(m, J_\alpha, \omega)$, and hence the dispersion function $\epsilon(\omega)$, are defined for positive and large enough $\mathrm{Im}(\omega)$. The continuation of $\epsilon(\omega)$ to the lower half-plane requires the continuation of functions such as

$$F^{(m)}_{\bar{c}c}(\omega) = \frac{1}{2\pi}\sum_\alpha \int\int_{V_\alpha} \frac{m f'_{0,\alpha}(J_\alpha)}{m\Omega_\alpha(J_\alpha)-\omega}\bar{c}_{m,\alpha}(J_\alpha)\cos\theta_\alpha \mathrm{e}^{\mathrm{i}mw_\alpha}\,\mathrm{d}w_\alpha\,\mathrm{d}J_\alpha. \tag{33}$$

The other integrals entering in $\epsilon(\omega)$ are similar, and hence we concentrate now on $F^{(m)}_{\bar{c}c}(\omega)$. We separately consider the integrals for different regions V_α, and introduce

$$\begin{aligned} F^{(m)}_{\bar{c}c,\alpha}(\omega) &= \frac{1}{2\pi}\int\int_{V_\alpha} \frac{m f'_{0,\alpha}(J_\alpha)}{m\Omega_\alpha(J_\alpha)-\omega}\bar{c}_{m,\alpha}(J_\alpha)\cos\theta_\alpha \mathrm{e}^{\mathrm{i}mw_\alpha}\,\mathrm{d}w_\alpha\,\mathrm{d}J_\alpha \\ &= \frac{1}{2\pi}\int_{J_\alpha^{(0)}}^{J_\alpha^{(1)}} \frac{m f'_{0,\alpha}(J_\alpha)}{m\Omega_\alpha(J_\alpha)-\omega}|c_{m,\alpha}(J_\alpha)|^2\,\mathrm{d}J_\alpha, \end{aligned} \tag{34}$$

where

$$J_1^{(0)} = J_3^{(0)} = 4\sqrt{M_0}/\pi, \qquad J_1^{(1)} = J_3^{(1)} = +\infty, \qquad J_2^{(0)} = 0, \qquad J_2^{(1)} = 8\sqrt{M_0}/\pi.$$

The $F^{(m)}_{\bar{c}c,\alpha}(\omega)$ are naturally defined by formula (34) for $\mathrm{Im}(\omega) > 0$. We need to define $F^{(m)}_{\bar{c}c,\alpha}(\omega)$ for $\mathrm{Im}(\omega) \leq 0$. When ω crosses the real axis, real roots of the equations $m\Omega_\alpha(J_\alpha) - \omega = 0$ create singularities. These singularities have to be dealt with using the usual Landau prescription: when the root $J_{\alpha,r}$ of the equation $\Omega_\alpha(J_{\alpha,r}) = \omega/m$ crosses the integration path, one takes the corresponding residue contribution. This procedure allows the analytic continuation of $F^{(m)}_{\bar{c}c,\alpha}(\omega)$ in the lower half-plane.

However, the continued dispersion function $\epsilon(\omega)$ has an infinite number of branch point singularities in the ω-plane. To see this, consider ω_1 in the upper half-plane, ω_2 in the lower half-plane, and a path in the ω-plane going from ω_1 to ω_2. Some examples of paths are shown in figure 3 for $\alpha = 2$ with corresponding paths on the J_2-plane. The number of times that the corresponding path crosses the integration path on the J_2-plane, and the orientation with which it crosses (from upper to lower half-plane, or from lower to upper half-plane) depends on the path which is chosen between ω_1 and ω_2. Consequently, the value of $F^{(m)}_{\bar{c}c,2}(\omega)$ depends on the choice of a continuation path, and each $\omega = m\omega_0$, where $\omega_0 = \lim_{J_2\to+0}\Omega_2(J_2)$ and $m \in \mathbb{Z}$, is a branch point of logarithmic type. See appendix D for more detailed explanations of the type of singularity. Because of these logarithmic branch points, we need an infinite number of Riemann sheets in ω to completely describe the dispersion function $\epsilon(\omega)$. The singularity structure of $F^{(m)}_{\bar{c}c,2}(\omega)$ is illustrated in figure 4, where two choices for the branch cuts are given.

The previous reasoning shows that $F^{(m)}_{\bar{c}c,\alpha}(\omega)$ has branch point singularities at the lower and upper boundaries of the range of the function $m\Omega_\alpha(J_\alpha)$. The ranges of Ω_1 and of Ω_3 are $(0, +\infty)$, and the only branch point is hence at $\omega = 0$ for $F^{(m)}_{\bar{c}c,1}(\omega)$ and $F^{(m)}_{\bar{c}c,3}(\omega)$. The range of Ω_2 is $(0, \omega_0)$, and there are two branch points at $\omega = 0$ and $m\omega_0$ for $F^{(m)}_{\bar{c}c,2}(\omega)$. With similar arguments, one may show that there are branch points also at

J. Stat. Mech. (2010) P08002

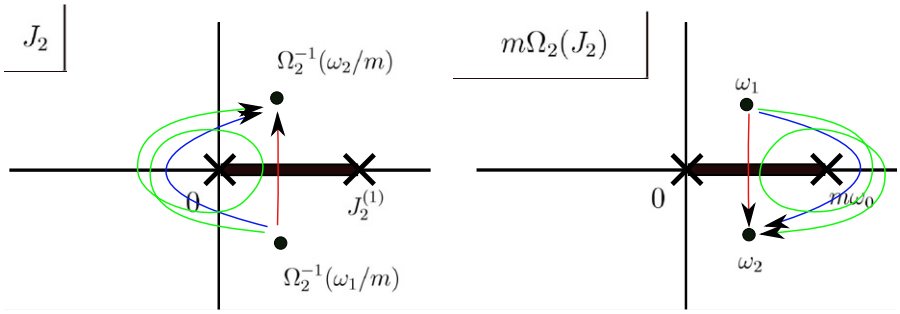

Figure 3. Examples of continuation paths from ω_1 to ω_2 on the $m\Omega_2(J_2)$-plane (right panel), and corresponding paths on the J_2-plane (left panel). The thick lines represent the interval of integration and its image under $m\Omega_2$. $J = 0$ and $J_2^{(1)}$ go to $m\Omega_2(0) = m\omega_0$ and 0 respectively under the mapping $m\Omega_2(J_2)$. This picture is for $m > 0$.

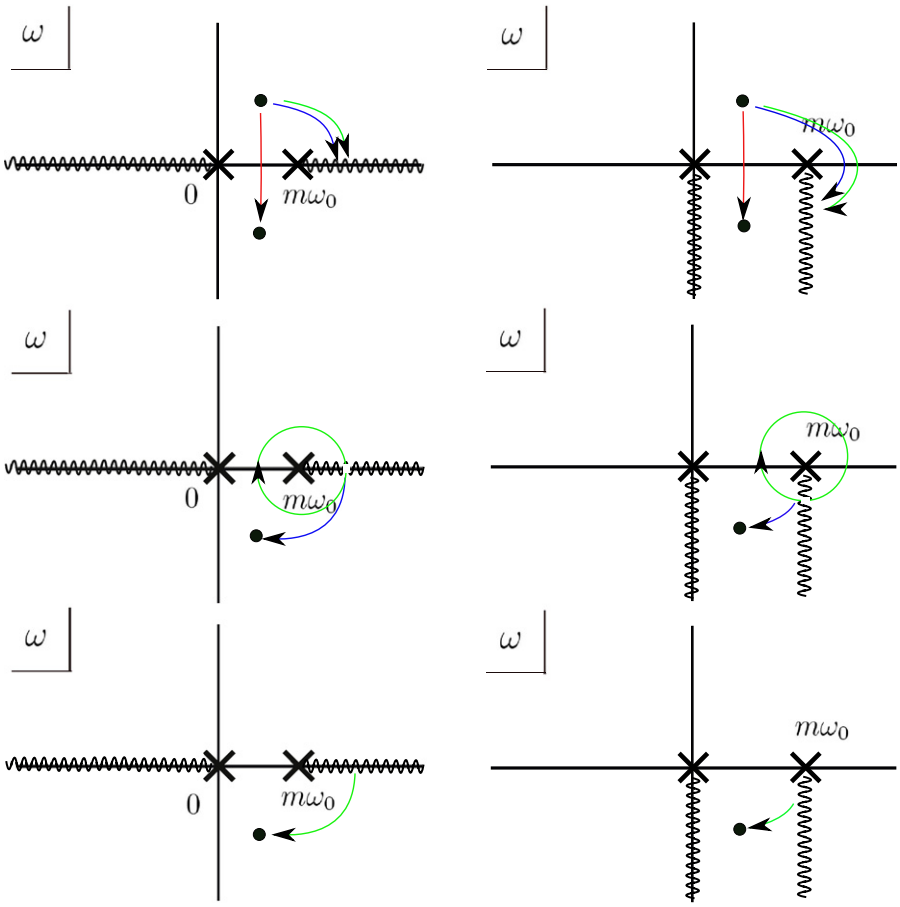

Figure 4. Two choices of branch cuts on the ω-plane for obtaining the analytic continuation of $F_{\bar{c}c,2}^{(m)}(\omega)$ for the lower half of the ω-plane. Each column represents a part of the Riemann surface of ω, for the logarithmic branch point $m\omega_0$. The three paths shown in figure 3 bring a point on the upper half-plane to three points on different Riemann sheets. The value of $F_{\bar{c}c,2}^{(m)}(\omega)$ at each of the three points is independent of the choice of the branch cuts.

J. Stat. Mech. (2010) P08002

the ω corresponding to stationary points of the frequency, that is points $\omega_c = m\Omega_\alpha(J_{\alpha,c})$, such that $(\mathrm{d}\Omega_\alpha/\mathrm{d}J_\alpha)(J_{\alpha,c}) = 0$. We will not have to deal with this case in the following, since no such real stationary points exist in the HMF model, as shown on figure 2.

4. Examples; comparison with N-body simulations

In this section, we compare the analytical results with dynamical simulations of N particles governed by the canonical equations of motion derived from Hamiltonian (1) for two families of stationary states. The dynamics of a perturbation $f_{1,\alpha}$ is theoretically obtained by the inverse Laplace transformation of $\hat{f}_{1,\alpha}$. For instance, each root of $\epsilon(\omega)$ gives an exponential contribution, and one may expect branch cuts to give algebraic contributions [30]. For simplicity, we focus on the contribution from the root of $\epsilon(\omega)$ whose imaginary part is the largest. The resulting exponential behavior cannot explain the dynamics of $f_{1,\alpha}$ perfectly, since it neglects the contributions from other roots and from branch cuts. However, in spite of this simplification, the root with the largest imaginary part captures some features of the growing or damping rates and frequency.

As explained in the introduction, the Vlasov dynamics approximates the N-particle dynamics; more precisely, they stay close to one other over a timescale $t_v(N)$ which diverges with N [1, 2] (the 'closeness' of these two dynamics may be defined in a rigorous manner). On the basis of [35] and the discussion in [36], we expect the timescale t_v to grow logarithmically with N when the initial conditions are close to an unstable stationary state of the Vlasov equation, and to grow at least algebraically with N when the initial conditions are close to a stable stationary state of the Vlasov equation. The Vlasov dynamics does not depend on N, and hence we can check that N is large enough for the Vlasov approximation to be valid by observing that the N-particle dynamics is independent of N over the timescale considered.

4.1. The water-bag stationary state

We consider first water-bag stationary states, which have a constant density in phase space up to a certain action, or energy, and a zero density beyond. The precise definition is as follows:

$$f_0(\theta, p) = \begin{cases} \eta_0 & \text{if } h_0(\theta, p) \leq E^*, \\ 0 & \text{if } h_0(\theta, p) > E^*, \end{cases} \tag{35}$$

where η_0 is determined by the normalization condition

$$\int\int_\mu f_0(\theta, p)\, \mathrm{d}\theta\, \mathrm{d}p = 1. \tag{36}$$

Note that f_0 determines the magnetization M_0, and that the energy E^* depends on M_0. Thus M_0 must obey a consistency equation. As a result, there exists a unique water-bag distribution such as (35) for each $M_0 \in [0, 1]$. It is important to note that E^* may be larger or smaller than the separatrix energy; this means the water-bag may be included inside the separatrix or not. We find that for $M_0 > M_0^{(s)} \simeq 0.33$, the water-bag is included inside the separatrix; for $M_0 < M_0^{(s)}$, it is not. We study in this section this one parameter family of distributions, computing the dispersion relation (31) and looking for

J. Stat. Mech. (2010) P08002

roots. Note that inhomogeneous water-bag solutions for an HMF model with anisotropy have been considered in [36]. In this reference, their stability is investigated, using a different method. The stability of water-bag distributions has also been investigated in the context of beam physics, where they are called Kapchinsky–Vladimirsky distributions; see for instance [37] and [38], where the stability is studied computing the evolution of moments of the distribution function.

Contrary to what happens with more general f_0, the integration over J does not create any singularity for $\omega \in \mathbb{R}$, thanks to the δ function included in f_0'. It results in a function $\epsilon(\omega)$ which only has poles for $\omega \in \mathbb{Z}\Omega_\alpha(J_\alpha^*)$, where J_α^* is the action corresponding to E^* with a suitable choice of α. Thus, the analytic continuation of the dispersion relation to the lower half of the ω-plane does not contain any branch cut singularity.

Solving $\epsilon(\omega) = 0$, varying the magnetization M_0 of the water-bag, we find that there exists a critical magnetization $M_0^{(c)} \simeq 0.37$ such that:

- for $M_0 < M_0^{(c)}$, the initial distribution is exponentially unstable: in this case, there exists at least one purely imaginary root of $\epsilon(\omega) = 0$, with positive imaginary part, that we call $\gamma(M_0)$;
- for $M_0 > M_0^{(c)}$, it is marginally stable: there exists in this case a discrete countable infinite number of real roots of $\epsilon(\omega) = 0$, $\omega_n = \omega_{n,r} + \mathrm{i}\omega_{n,i}$, with $\omega_{n,i} = 0$; we name as $\omega_{1,r}(M_0)$ the smallest of these frequencies.

These features are not unexpected: it is known that homogeneous stationary states of the Vlasov equation with compact support in velocity may sustain undamped oscillating discrete modes (see [39] for examples with the HMF model). The same type of phenomenon occurs for 1D self-gravitating systems [16]–[18], and vortices (see for instance [21]). We have shown that such undamped modes exist in the case of inhomogeneous water-bag stationary states of the Vlasov equation. More surprising is the behavior of the growing rate $\gamma(M_0)$: it has a complicated behavior around $M_0 = M_0^{(s)}$; see figure 5.

We have performed direct N-body numerical simulations, adding a small perturbation to the initial phase space distribution (35):

$$f(\theta, p, t = 0) = \begin{cases} \eta_0' & \text{if } h_0(\theta, p) \leq E^*(1 + a\cos\theta), \\ 0 & \text{if } h_0(\theta, p) > E^*(1 + a\cos\theta), \end{cases} \tag{37}$$

where η_0' is determined by the normalization condition (36). In the unstable case, $M(t)$ rapidly grows as shown in figure 6. There is no dependence on N, and hence the Vlasov approximation is valid in this short time region, although the agreement between $N = 10^6$ and 10^7 becomes worse as M_0 decreases. We fit the evolution of $M(t)$ with a pure exponential, and extract a growing rate; it is in qualitative agreement with the analytically computed growing rate $\gamma(M_0)$, except around $M_0^{(s)}$. We remark that $M(t)$ is not simply exponential. The quantitative agreement is hence not very good, as shown in figure 5. In the stable case, the numerically computed $M(t)$ is oscillating and shows no sign of damping, in agreement with the theory; the fitted frequency is very close to the analytically computed $\omega_1(M_0)$ as reported in figure 7. In this stable case also, the temporal evolutions of $M(t)$ for $N = 10^6$ and 10^7 coincide up to $t = 50$, except when M_0 is close to the critical value $M_0^{(c)}$; the frequency has no dependence on N.

J. Stat. Mech. (2010) P08002

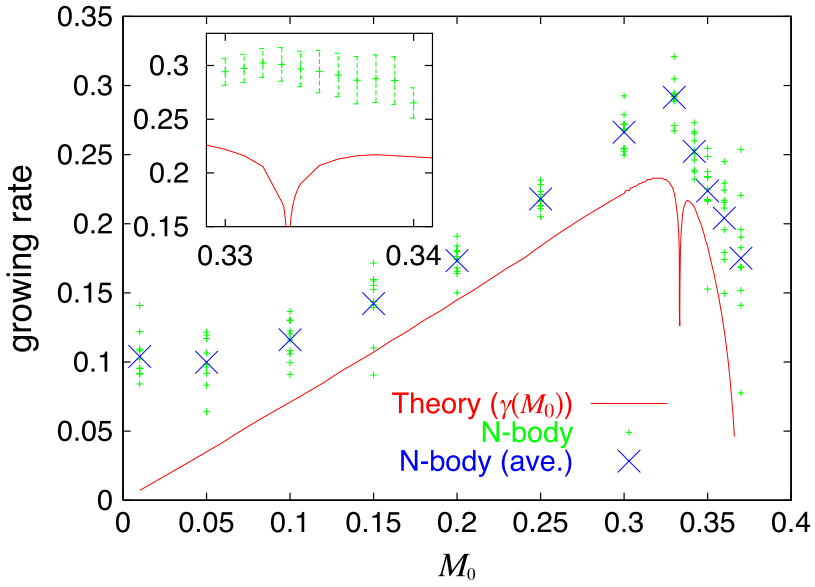

Figure 5. Growing rates for an unstable inhomogeneous water-bag background. The red line represents $\gamma(M_0)$, labeled as theory. Green points are estimations of the growing rates by N-body simulations for 10 realizations at each value of M_0, and the big blue crosses are the averages over the 10 realizations. The perturbation amplitude a (see (37)) is chosen as $a = 0.01$ for $M_0 < 0.15$ and $a = 0.001$ otherwise. The inset is a magnification around $M_0^{(s)}$. Green points are averages over 40 realizations, and error bars represent the standard deviations. There is no signature of the dip at $M_0^{(s)}$ which is predicted by the theory.

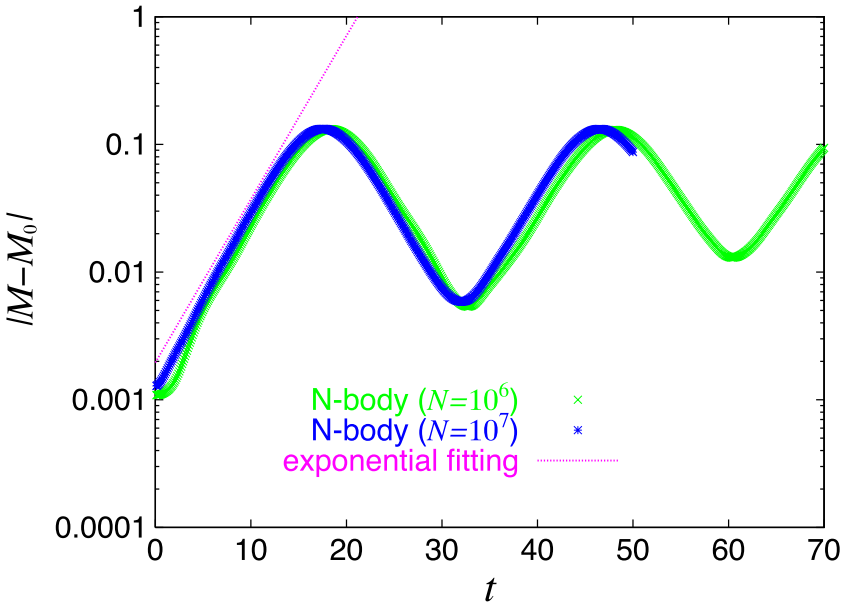

Figure 6. Temporal evolution of $M(t)$ for an unstable water-bag, and estimation of the growing rate. $M_0 = 0.33$. $a = 0.001$. $N = 10^6$ and 10^7.

doi:10.1088/1742-5468/2010/08/P08002

J. Stat. Mech. (2010) P08002

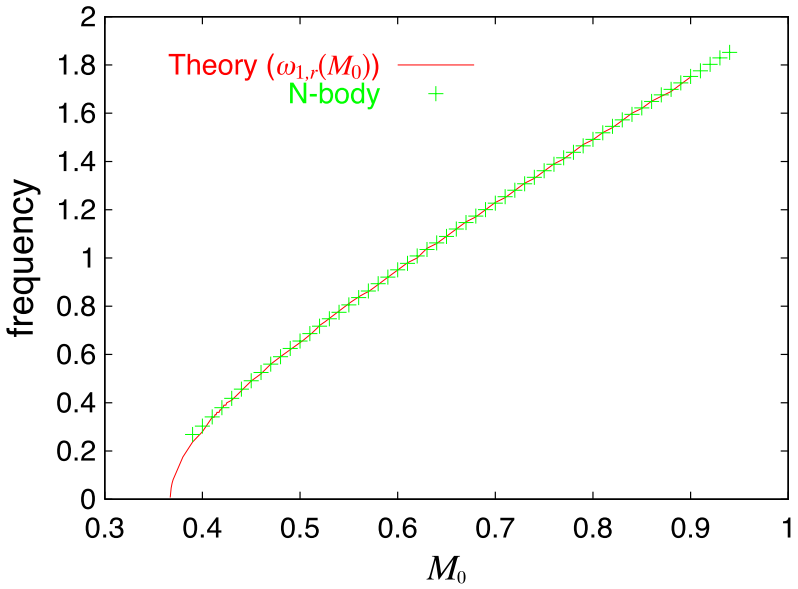

Figure 7. Oscillation frequencies for a perturbation around a stable inhomogeneous water-bag background. The red line represents $\omega_{1,r}(M_0)$, labeled as theory. Green points are the frequencies extracted from a single realization of the dynamics by N-body simulations with $N = 10^6$ particles. The latter correspond to a peak in the power spectrum of $M(t)$, which is computed from the interval $0 \leq t \leq 1638.4$.

4.2. Thermal equilibrium

We turn now to stationary states corresponding to thermal equilibria, parameterized by the temperature $T = 1/\beta$:

$$f_0(\theta, p) = \mathcal{N} \mathrm{e}^{-\beta(p^2/2 - M_0 \cos\theta)} \tag{38}$$

where $\mathcal{N}$ is the normalization and the magnetization $M_0(T)$ is solution to the consistency equation. The thermodynamical equilibrium state of the HMF is inhomogeneous (that is $M_0 \neq 0$) as soon as $T < 0.5$ [34].

For such an initial distribution, the general results of section 3 concerning the analytical continuation of $\epsilon(\omega)$ apply. To fully describe the behavior of the magnetization $M(t)$ one would in principle need to compute the inverse Laplace transform of Σ_C and Σ_S computed from (30). This usually requires the deformation of the Bromwich contour in the complex ω-plane. One may expect a contribution to the function $M(t)$ from the generalization of the 'Landau poles', that is the roots of $\epsilon(\omega)$. However, because of the complicated analytic structure of the integrand, a careful analysis of the inverse Laplace transform is needed, which is beyond the scope of the present paper. In the following, we will identify the roots of $\epsilon(\omega)$, pick out $\omega_L(T)$, the root with the largest imaginary part, and see whether this root gives hints for understanding the N-body numerical simulations. The initial distribution f_0 is stable for $T < 0.5$, and hence all such roots are in the lower half of the ω-plane. We stress that in principle, we cannot expect a perfect agreement between the numerical $M(t)$ and the contribution of $\omega_L(T)$. To look for roots of $\epsilon(\omega)$, we

J. Stat. Mech. (2010) P08002

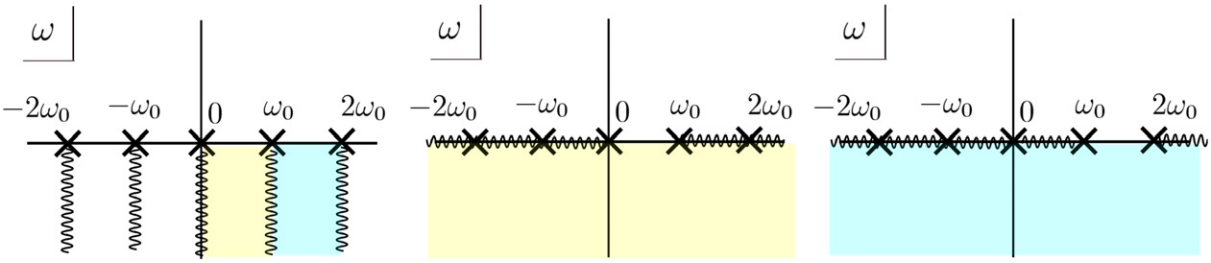

Figure 8. Three choices of branch cuts, which are represented by wavy lines. In the three panels, one color identifies one Riemann sheet.

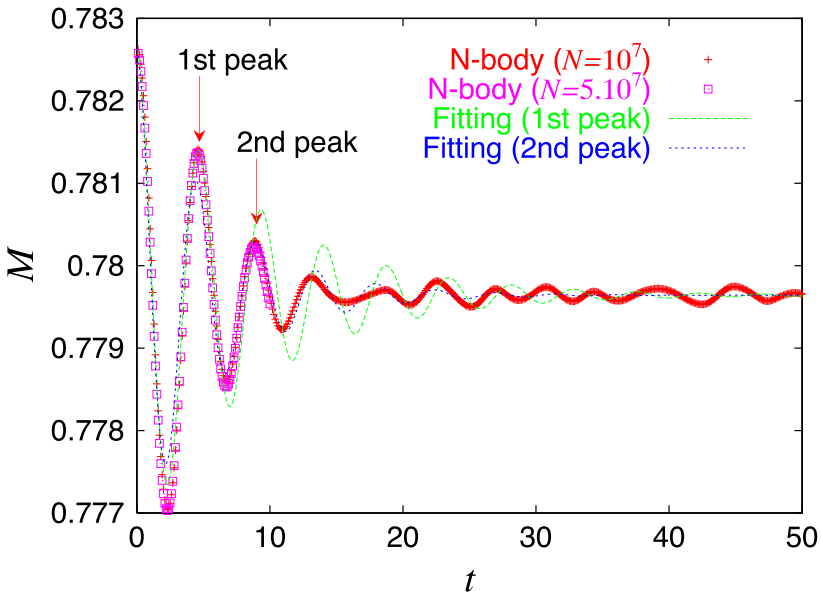

Figure 9. Temporal evolution of $M(t)$ for stable thermal equilibrium. $T = 0.3$. $a = 0.1$. $N = 10^7$ and 5×10^7.

have explored several choices of analytic continuation, or equivalently several Riemann sheets.

Three choices of branch cuts are sketched in figure 8. The numerical procedure for computing the dispersion relation, performing its analytical continuation and finding its roots is detailed in appendix E with an example of level curves for $|\epsilon(\omega)|$. It turns out that two different roots of $\epsilon(\omega)$ have the same imaginary part for $T \simeq 0.4$ and switching of $\omega_L(T)$ occurs. This is the origin of the non-monotonic and non-differentiable behavior of $-\mathrm{Im}(\omega_L)$, and the jump in $\mathrm{Re}(\omega_L)$ visible in figures 10 and 11.

We have performed the N-body simulations using the following perturbed thermal equilibrium initial distribution:

$$f(\theta, p, t = 0) = \mathcal{N}_a \mathrm{e}^{-\beta(p^2/2 - M_0 \cos\theta)}(1 + a\cos\theta). \tag{39}$$

A typical temporal evolution of $M(t)$ is shown in figure 9; $M(t)$ has no dependence on N, although the agreement between $N = 10^7$ and 5×10^7 deteriorates as T increases. $M(t)$

J. Stat. Mech. (2010) P08002

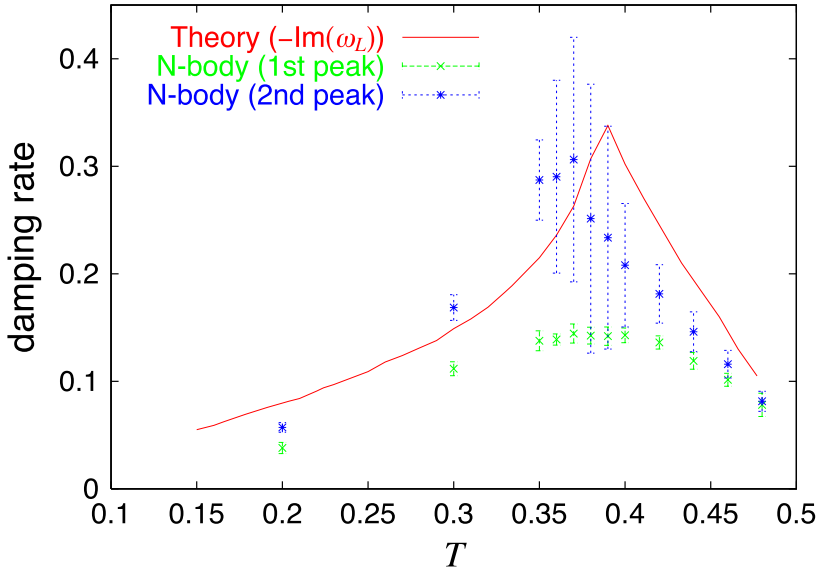

Figure 10. Estimated damping rate as a function of T. The red line represents $-\mathrm{Im}(\omega_L)$, labeled as theory. In N-body simulations, for each value of T, the damping rates are estimated for 20 realizations, and their average and standard deviation are reported by a point and the error bar around it respectively. The symbols for first and second peaks represent the rate estimated by using the first and second peaks of $M(t)$ respectively. $N = 10^7$.

shows a damped oscillation, which is assumed as to be in the form of

$$M(t) = A + B\mathrm{e}^{-\lambda t}\cos\nu t. \tag{40}$$

We assumed that $M(t)$ has a maximum at $t = 0$ from the given perturbation.

We perform the following procedure to estimate the values of A, B, λ and ν for each orbit. $M(t)$ relaxes to the equilibrium value, and A is computed by time averaging in the interval $20 < t \leq 50$. The initial amplitude of oscillation B is computed as $M(0) - A$. To estimate λ and ν, we pick out the peaks $M(t_j)$, where t_j is the time at which $M(t)$ has its jth peak, with the zeroth peak defined as the peak at $t = 0$. For the jth peak, we can estimate $\nu = 2\pi/t_j$ and $\lambda = \ln((M(0) - A)/(M(t_j) - A))/t_j$. The values of λ and ν which should be compared to $-\mathrm{Im}(\omega_L)$ and $\mathrm{Re}(\omega_L)$ are reported in figures 10 and 11 respectively; each figure shows the values estimated from the first and second peaks.

To be precise, the assumption (40) is not valid since the values of λ and μ change if we change the choice of the peak. This means that the damping is indeed not simply exponential, and that the Landau pole ω_L does not provide a complete description of the damped oscillation. However, the Landau pole ω_L seems to capture the tendencies of the dependence on T, including around $T = 0.4$.

5. Discussion and conclusion

We have studied the linearized Vlasov equation around an inhomogeneous stationary state, and computed the associated dispersion function $\epsilon(\omega)$. We have shown that $\epsilon(\omega)$ generically has an infinite number of branch points associated with logarithmic

J. Stat. Mech. (2010) P08002

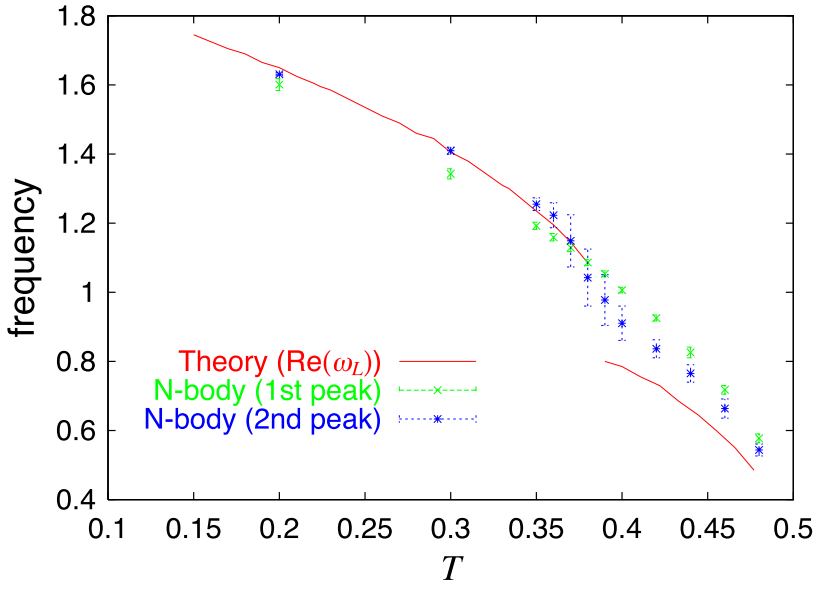

Figure 11. The same as figure 10, but where the estimated value is the frequency. The red discontinuous line represents $\mathrm{Re}(\omega_L)$, labeled as theory. Note the jump around $T = 0.4$.

singularities, and thus an infinite number of possible analytic continuations in the lower half-plane. Although we have studied here the HMF model, it is safe to conjecture that the singularity structure that we have found for the dispersion function $\epsilon(\omega)$ does not depend on the precise model, at least in 1D. Indeed, the branch points come from the existence of lower or upper bounds for the range of the frequency Ω. These singularities make the situation much more complicated in the inhomogeneous case than in the usual homogeneous one. We note however that, to our knowledge, these branch cuts have not been exploited or pointed out in the literature on stellar systems (see for instance [14, 41]); their existence is likely, and the question of their possible relevance is open.

We have studied in detail two special classes of inhomogeneous stationary states: the water-bags and the thermal equilibria. The comparison between direct N-body numerical simulations and the roots of the dispersion relation $\epsilon(\omega) = 0$ is satisfactory for water-bags, but we note that water-bags are very special distributions, for which ϵ does not present branch cuts. For thermal equilibria, although the analysis of the roots of $\epsilon(\omega) = 0$ gives useful hints for understanding the dynamics of the system, we find qualitative discrepancies with a simple 'Landau-like' damping. This feature was to be expected, given the complicated analytical structure of $\epsilon(\omega)$.

This study leaves open several questions: Is it possible to understand better the long time behavior of the linearized Vlasov equation by taking into account all contributions in the inverse Laplace transform, in the spirit of [30]? When the damping is very weak, is there a phenomenon analogous to the 'quasimodes' in hydrodynamics [21]? This question necessitates a study of the eigenfunctions of the problem, for stationary states other than water-bags and thermal equilibria. When the damping is weak enough and the perturbation strong enough, is there a phenomenon similar to nonlinear Landau damping [7]?

J. Stat. Mech. (2010) P08002

Finally, we stress the following technical point: we have shown that the linearized Vlasov equation is particularly simple for the HMF model, since the final matrix equation is diagonal. This may make the HMF model particularly well suited for developing, and testing in numerical experiments, a kinetic theory including all collective effects, thus going beyond that of [4].

Acknowledgments

This work was supported by the Ministry of Education, Science, Sports and Culture, Grant-in-Aid for Young Scientists (B), 19760052, and by the ANR-09-JCJC-009401 INTERLOP project. YYY acknowledges an invited professorship at Nice Sophia-Antipolis University in August–September 2009. Computations were partially performed on the 'Mésocentre SIGAMM' machine, hosted by the Observatoire de la Côte d'Azur. We acknowledge discussions with F Bouchet and H Morita, and thank a referee for many useful suggestions.

Appendix A. Elliptic integrals and elliptic functions

We review the definitions and features of the Legendre elliptic integrals and the Jacobian elliptic functions, which are used to introduce angle–action variables in the pendulum system.

The Legendre elliptic integrals of the first and second kinds are defined by

$$F(\phi,k)=\int_0^\phi \frac{\mathrm{d}\theta}{\sqrt{1-k^2\sin^2\theta}},\qquad E(\phi,k)=\int_0^\phi \sqrt{1-k^2\sin^2\theta}\,\mathrm{d}\theta \tag{A.1}$$

respectively. Both the first kind and the second kind are odd with respect to ϕ. The complete elliptic integrals of the first and second kinds are defined by setting $\phi=\pi/2$ as

$$K(k)=F(\pi/2,k),\qquad E(k)=E(\pi/2,k) \tag{A.2}$$

respectively. We remark that $K(0)=E(0)=\pi/2$, $E(1)=1$ and $K(1)$ diverges.

The Jacobian elliptic function sn is defined as the function such that

$$\mathrm{sn}(F(\phi,k),k)=\sin\phi. \tag{A.3}$$

Other Jacobian elliptic functions cn and dn are defined from sn as

$$\mathrm{cn}(z,k)=\sqrt{1-\mathrm{sn}^2(z,k)},\qquad \mathrm{dn}(z,k)=\sqrt{1-k^2\mathrm{sn}^2(z,k)}, \tag{A.4}$$

where the branches of the square root are chosen such that $\mathrm{cn}(0,k)=1$ and $\mathrm{dn}(0,k)=1$.

Appendix B. Angle–action variables for the pendulum

With the choice of the potential phase $\psi=0$ the potential $\phi[f_0](\theta,t)$ (5) is rewritten as

$$\phi[f_0](\theta,t)=-M_0\cos\theta,$$

where M_0 is the magnetization of the stationary state f_0, which depends only on the one-particle energy (8). The one-particle Hamiltonian (8) is hence the same as that of the

pendulum expressed by the Hamiltonian

$$H(\theta, p) = \tfrac{1}{2}p^2 - M_0 \cos\theta. \tag{B.1}$$

We introduce angle–action variables (w, J) in the pendulum system.

The action J is generally defined by

$$J = \frac{1}{2\pi} \oint p \, \mathrm{d}\theta, \tag{B.2}$$

where the momentum p is a function of θ and energy h:

$$p = \pm\sqrt{2(h + M_0 \cos\theta)}.$$

Performing the integration of (B.2), the action variable J_α defined in U_α is expressed as

$$\begin{aligned} J_1 &= \frac{4\sqrt{M_0}k}{\pi} E(1/k), \qquad (\theta, p) \in U_1 \\ J_2 &= \frac{8\sqrt{M_0}}{\pi} [E(k) - (1 - k^2)K(k)], \qquad (\theta, p) \in U_2 \\ J_3 &= \frac{4\sqrt{M_0}k}{\pi} E(1/k), \qquad (\theta, p) \in U_3 \end{aligned} \tag{B.3}$$

where $K(k)$ and $E(k)$ are the complete elliptic integrals of the first and second kinds respectively, and

$$k = \sqrt{\frac{h + M_0}{2M_0}}.$$

The angle variable w is obtained through a generator $W(\theta, J)$ of the canonical transformation $(\theta, p) \mapsto (w, J)$ as

$$w = \frac{\partial W}{\partial J}(\theta, J). \tag{B.4}$$

We define the generator as

$$W(\theta, J) = \int p(q, J) \, \mathrm{d}q; \tag{B.5}$$

then the angle variable w_α defined in U_α is written as

$$\begin{aligned} w_1 &= \pi \frac{F(\theta/2, 1/k)}{K(1/k)} \qquad (\theta, p) \in U_1 \\ w_2 &= \begin{cases} \dfrac{\pi}{2} \dfrac{F(\Theta, k)}{K(k)} & (\theta, p) \in U_2, \quad p \geq 0 \\ \dfrac{\pi}{2} \left(2 - \dfrac{F(\Theta, k)}{K(k)} \right) & (\theta, p) \in U_2, \quad p < 0 \end{cases} \\ w_3 &= -\pi \frac{F(\theta/2, 1/k)}{K(1/k)} \qquad (\theta, p) \in U_3, \end{aligned} \tag{B.6}$$

where Θ satisfies $k \sin\Theta = \sin(\theta/2)$. We defined w_2 to be continuous at the turning point $w_2 = \pi/2$. Accordingly the range of the angle variable is $-\pi < w_\alpha \leq \pi$ for $\alpha = 1, 3$ and $-\pi/2 < w_2 \leq 3\pi/2$.

J. Stat. Mech. (2010) P08002

Summarizing, we have introduced bijective transformations $\varphi_\alpha : U_\alpha \to V_\alpha$ where

$$\begin{aligned} V_1 &= (-\pi, \pi] \times (4\sqrt{M_0}/\pi, \infty), \\ V_2 &= (-\pi/2, 3\pi/2] \times (0, 8\sqrt{M_0}/\pi), \\ V_3 &= (-\pi, \pi] \times (4\sqrt{M_0}/\pi, \infty). \end{aligned} \tag{B.7}$$

These bijective transformations φ_α are canonical transformations from (θ, p) to (w_α, J_α), and hence $\mathrm{d}\theta \wedge \mathrm{d}p = \mathrm{d}w_\alpha \wedge \mathrm{d}J_\alpha$ holds.

The pendulum is integrable and hence the Hamiltonian $H(\theta, p)$ is a function of the action only, written as $H_\alpha(J_\alpha)$. The pendulum oscillates in U_2 and rotates in U_1 and U_3, and its frequency $\Omega_\alpha(J_\alpha)$ is obtained by

$$\Omega_\alpha(J_\alpha) = \frac{\mathrm{d}H_\alpha}{\mathrm{d}J_\alpha}(J_\alpha). \tag{B.8}$$

The frequency $\Omega_\alpha(J_\alpha)$ defined in U_α is computed as

$$\begin{aligned} \Omega_1(J_1) &= \frac{\pi\sqrt{M_0}k}{K(1/k)} \qquad (\theta, p) \in U_1, \\ \Omega_2(J_2) &= \frac{\pi\sqrt{M_0}}{2K(k)} \qquad (\theta, p) \in U_2, \\ \Omega_3(J_3) &= \frac{\pi\sqrt{M_0}k}{K(1/k)} \qquad (\theta, p) \in U_3. \end{aligned} \tag{B.9}$$

Using the symmetries in the definition of the action–angle variables, it is easy to prove the following relations for the $c_{m,\alpha}$ and $s_{m,\alpha}$ functions defined in (24):

$$c_{m,3}(J) = c_{m,1}(J); \qquad s_{m,3}(J) = -s_{m,1}(J), \tag{B.10}$$

$$c_{m,2}(J) = 0 \qquad \text{if } m \text{ odd}; \qquad s_{m,2}(J) = 0 \qquad \text{if } m \text{ even}. \tag{B.11}$$

The final remark concerns the continuity of the angle–action variables. For instance, the limits of J_α at the separatrix do not coincide:

$$\lim_{h \to h^{(s)} - 0} J_2 = 2 \lim_{h \to h^{(s)} + 0} J_1 = 2 \lim_{h \to h^{(s)} + 0} J_3,$$

with $h^{(s)}$ the separatrix energy; the limit $h \to h^{(s)} \pm 0$ is the same as the limit $k \to 1 \pm 0$. The difference of the factor 2 comes from the definition of the action, which represents the area surrounded by a closed orbit. The closed orbit goes to both upper *and* lower half-planes of p for $h < h^{(s)}$, but it goes to upper *or* lower half-planes for $h > h^{(s)}$. Similarly the limits of w_α at the separatrix do not coincide.

Appendix C. General potentials

The computations in section 2 are made easier by the special form of the HMF potential: the two-body interaction contains only one (complex) Fourier mode. As a consequence, the matrix equation (30) yielding the perturbation's potential is of size 2.

J. Stat. Mech. (2010) P08002

As a generic interaction potential with periodic boundary condition contains an infinite number of Fourier modes, the dispersion relation will appear as the determinant of an infinite-size matrix, and the perturbation's potential will be solution of an infinite-size matrix equation. In the HMF case, this matrix is actually diagonal. It is important to know whether this is a generic property or not.

The coefficients of the infinite matrix will contain the generalizations of the c_m and s_m functions:

$$c_{m,n}(J) = \int \cos(n\theta(w,J))\mathrm{e}^{\mathrm{i}mw}\,\mathrm{d}w; \qquad s_{m,n}(J) = \int \sin(n\theta(w,J))\mathrm{e}^{\mathrm{i}mw}\,\mathrm{d}w, \tag{C.1}$$

where w and J are the angle and action variables in the potential defined by the stationary state. Provided that this stationary state is symmetric under the reflexion $\theta \to -\theta$, it is easy to show that the $c_{m,n}$s and $s_{m,n}$s enjoy properties similar to (B.10) and (B.11). However, there is no reason that the non-diagonal terms of the matrix expression of the following type:

$$F_{\bar{c}c,nn'} = \sum_m \int \frac{mf_0'(J)}{m\Omega(J)-\omega}\bar{c}_{m,n}(J)c_{m,n'}(J)\,\mathrm{d}J \tag{C.2}$$

should vanish. The case of HMF is thus particularly simple.

We have considered until now only periodic potentials. For non-periodic potentials, one can no longer use the Fourier basis to expand the functions of the spatial variable. The trick is to use a doubly orthogonal family of functions to expand ϕ_1 and $\rho_1 = \int f_1\,\mathrm{d}p$. The dispersion relation is then obtained in a very similar way; see for instance [13].

Appendix D. Singularity of $F_{\bar{c}c}$ and $F_{\bar{s}s}$ around $\omega = m\omega_0$

To describe the singularity of $F^{(m)}_{\bar{c}c,2}(\omega)$ and $F^{(m)}_{\bar{s}s,2}(\omega)$ at $\omega = m\omega_0$, we consider the following integral:

$$\varphi(\omega) = \int_a^b \frac{g(J)}{h(J)-\omega}\,\mathrm{d}J \tag{D.1}$$

and suppose that the function $h(J)$ has no stationary point, and that its range is $[\alpha,\beta]$ where $\alpha = h(b)$ and $\beta = h(a)$. This setting covers the situation that we are interested in, with $g(J) = f_0'(J)|c_{m,2}(J)|^2$, and $h(J) = m\Omega_2(J)$. A change of variable $p = h(J)$ yields

$$\varphi(\omega) = -\int_\alpha^\beta \frac{g(h^{-1}(p))(h^{-1})'(p)}{p-\omega}\,\mathrm{d}p = -\int_\alpha^\beta \frac{\tilde{g}(p)}{p-\omega}\,\mathrm{d}p \tag{D.2}$$

where $\tilde{g}(p) = g(h^{-1}(p))(h^{-1})'(p)$. We are interested in the singularity of $\varphi(\omega)$ near $\omega = \beta$.

Suppose that $\varphi(\omega)$ is defined for $\mathrm{Im}(\omega) > 0$, and we want to perform the analytic continuation of $\varphi(\omega)$ to the whole ω-plane. Let r, θ_1 and θ_2 be real, with $0 < r < \beta - \alpha$. We move from $\omega_1 = \beta - r\mathrm{e}^{-\mathrm{i}\theta_1}$ with $\theta_1 > 0$ (so that ω_1 is in the upper half-plane) to $\omega_2 = \beta - r\mathrm{e}^{-\mathrm{i}\theta_2}$ with $\theta_2 < 0$ (in the lower half-plane), using one of the paths represented in figure 3. These paths are parameterized by $s \in [0,1]$:

$$L_0 : \theta(s) = (1-s)\theta_1 + s\theta_2 \qquad L_1 : \theta(s) = (1-s)\theta_1 + s(\theta_2 + 2\pi)$$
$$L_2 : \theta(s) = (1-s)\theta_1 + s(\theta_2 + 4\pi).$$

The path L_1 does not cross the integration interval, so no residue contribution appears. The path L_0 crosses the integration interval once from the upper to the lower side, and hence the residue of the singular point, $\omega = \beta - r\mathrm{e}^{-\mathrm{i}\theta_2}$, positively contributes to $\varphi(\omega)$. The path L_2 crosses the integration interval once from the lower to the upper side, so the residue negatively contributes to $\varphi(\omega)$.

One may of course consider similarly other paths, and hence the analytic continuation gives

$$\varphi(\omega; n) = -P\int_\alpha^\beta \frac{\tilde{g}(p)}{p-\omega}\,\mathrm{d}p + 2\pi\mathrm{i}(1-n)\tilde{g}(\omega) \tag{D.3}$$

where P represents the principal value, and n the path chosen:

$$L_n : \theta(s) = (1-s)\theta_1 + s(\theta_2 + 2\pi n).$$

Consequently, the branch point $\omega = \beta$ has a logarithmic type singularity. We remark that the singularity comes from the existence of the upper boundary of the range of $h(J)$.

Now, to describe more precisely the singularity, we expand $\tilde{g}$ around $p = \beta$ as $\tilde{g}(p) = c(p-\beta)^n$, with n an integer. Then it is easy to check by direct integration that $\varphi(\omega)$ has a branch point for $\omega = \beta$, and that the singularity is of the type $\varphi(\omega) = (\omega-\beta)^n \ln(\omega-\beta)$.

To apply the previous result to $F^{(m)}_{\bar{c}c,2}(\omega)$ and $F^{(m)}_{\bar{s}s,2}(\omega)$, we need to expand $c_{m,2}(J_2)$ and $s_{m,2}(J_2)$ in powers of J_2. For this purpose, we will use the variable $k = \sqrt{(h+M_0)/2M_0}$ rather than J_2; close to $k=0$, we have $J_2 = \mathrm{O}(k^2)$. In an abuse of notation, we will keep the same name for the functions $c_{m,2}(k)$ and $s_{m,2}(k)$. We use now the following expressions, obtained from (B.6):

$$c_{m,2}(k) = \int_{-\pi}^{\pi}\left[1 - 2k^2\mathrm{sn}^2\left(\frac{2}{\pi}K(k)w, k\right)\right]\mathrm{e}^{\mathrm{i}mw}\,\mathrm{d}w \tag{D.4}$$

$$s_{m,2}(k) = \int_{-\pi}^{\pi} k\,\mathrm{sn}\left(\frac{2}{\pi}K(k)w, k\right)\mathrm{dn}\left(\frac{2}{\pi}K(k)w, k\right)\mathrm{e}^{\mathrm{i}mw}\,\mathrm{d}w. \tag{D.5}$$

We essentially need to know the Fourier coefficients of the sn and dn functions appearing in the above expressions, which are 2π periodic functions of w_2. These Fourier coefficients are given by the series expansions [40]

$$\mathrm{sn}(u,k) = \frac{2\pi}{kK(k)}\sum_{n=0}^{+\infty}\frac{q^{n+1/2}}{1-q^{2n+1}}\sin\left[(2n+1)\frac{\pi u}{2K(k)}\right] \tag{D.6}$$

$$\mathrm{dn}(u,k) = \frac{\pi}{2K(k)} + \frac{2\pi}{K(k)}\sum_{n=0}^{+\infty}\frac{q^n}{1+q^{2n}}\cos\left[2n\frac{\pi u}{2K(k)}\right] \tag{D.7}$$

where $q(k) = k^2/16 + \mathrm{O}(k^4)$. Collecting the various contributions, one finally finds that close to $k=0$,

$$c_{m,2}(k) = \mathrm{O}(k^m) \qquad \text{if } m \text{ even}; \qquad s_{m,2}(k) = \mathrm{O}(k^m) \qquad \text{if } m \text{ odd}. \tag{D.8}$$

Recall that $c_{m,2} = 0$ for odd m, and $s_{m,2} = 0$ for even m. Now $\lim_{J_2\to+0}\Omega_2'(J_2) = -c$, with $c > 0$, and generically $f_0'(J=0) \neq 0$. Then putting together the previous expressions, we

conclude that

$$F^{(m)}_{\bar{c}c,2}(\omega) \sim \text{const.} \times (\omega - m\omega_0)^m \ln(\omega - m\omega_0) \qquad \text{if } m \text{ even}, \tag{D.9}$$

$$F^{(m)}_{\bar{s}s,2}(\omega) \sim \text{const.} \times (\omega - m\omega_0)^m \ln(\omega - m\omega_0) \qquad \text{if } m \text{ odd}. \tag{D.10}$$

In particular the singularity becomes weaker and weaker for increasing m. The singularity at $\omega = 0$ is more complicated to analyze. We do not study it in this paper.

Appendix E. Finding roots of $\epsilon(\omega)$

In order to evaluate $F_{\bar{c}c}$ and $F_{\bar{s}s}$ in (31), we have to compute the integrals in expressions (29) and add the residue contributions. For this latter part, we need to compute complete elliptic integrals and Jacobian elliptic functions in the whole complex plane (these functions appear in the expressions for Ω_α, $c_{m,\alpha}$ and $s_{m,\alpha}$). For this purpose, we use their expressions in terms of theta functions, and refer the reader to [42]–[45].

E.1. Pole contributions

We need to find the roots J^*_α of $m\Omega_\alpha(J_\alpha) - \omega$ for all $m \in \mathbb{Z}$ and $\omega = \omega_r + \mathrm{i}\omega_i \in \mathbb{C}$.

First, for each α, m and ω, we are able to show that there is only one quadrant of the J-plane where one or several roots may exist. This helps with the numerical root finding procedure, and is also important for understanding the sign of the residue contribution to $F^{(m)}_{\bar{c}c,\alpha}$ when ω crosses the real axis.

Then, we look for the minima of $|m\Omega_\alpha(J_\alpha) - \omega|$ which are equal to zero. Numerically, we use the Simplex algorithm of Nelder and Mead, included in the GNU Scientific Library (GSL), with a grid of initial conditions distributed in the candidate quadrant. In all cases and for each α, we find exactly one zero, and all initial conditions of the minimization procedure yield the same result.

The last step is to compute the residue associated with J^*_α, multiplied by $\pm 2\mathrm{i}\pi$, depending on how J^*_α crosses the real axis when ω crosses the real axis (from the upper half-plane to the lower one, or from the lower to the upper one).

Finally, we truncate the sum over $m \in \mathbb{Z}$ at ± 5. Going further did not change the results, up to our numerical precision.

E.2. Integral parts of $F_{\bar{c}c}$ and $F_{\bar{s}s}$

Apart from finding the residue contributions, the computation of $F_{\bar{c}c}$ and $F_{\bar{s}s}$ is based mainly on several unidimensional integrations. To perform them we typically used the adaptive integration QAG and QAGIU routines based on Gauss–Kronrod rules included in the GSL library. The first one considers a bounded domain (it is the case in the U_2 region) whereas the second one integrates over a semi-infinite interval (it is the case in the U_1 and U_3 regions).

To avoid any integration problem due to the singularity at the separatrix J_s, we cut the integration domain at a distance ϵ from J_s. We choose ϵ so that it does not modify the results up to our numerical precision, set to 10^{-5} for the absolute error and 10^{-4} for the

J. Stat. Mech. (2010) P08002

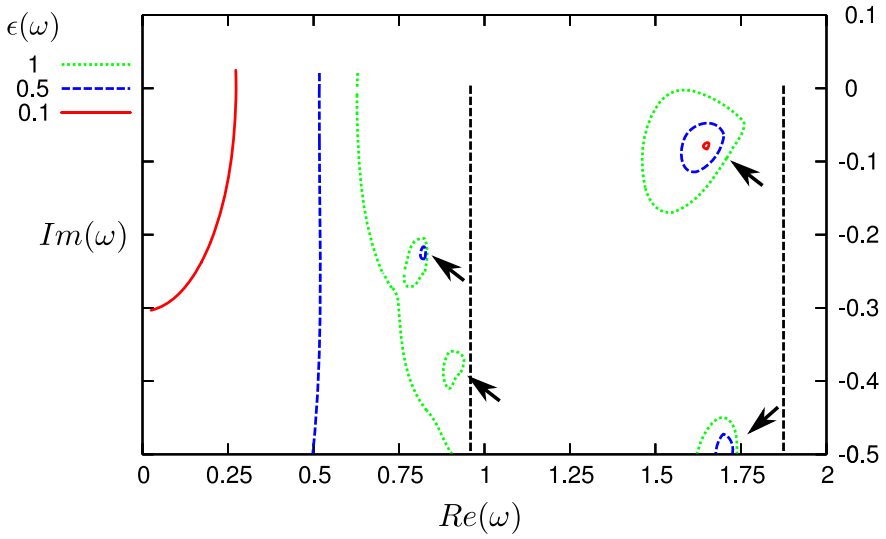

Figure E.1. Level curves of $|\epsilon(\omega)|$ for thermal equilibrium with $T = 0.2$. Vertical dashed black lines represent branch cuts. Regions where roots may exist are indicated by arrows.

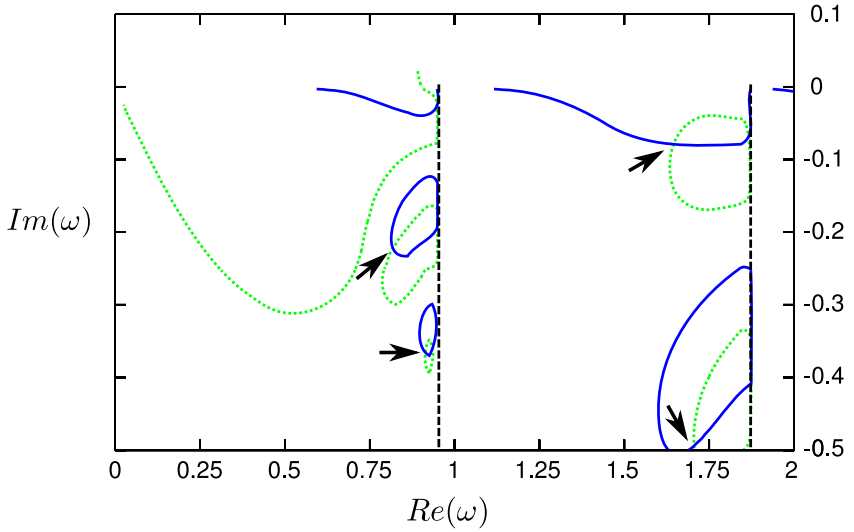

Figure E.2. Level curves of $\mathrm{Re}(\epsilon(\omega)) = 0$ (straight blue line) and $\mathrm{Im}(\epsilon(\omega)) = 0$ (dotted green line) for thermal equilibrium with $T = 0.2$. Vertical dashed black lines represent branch cuts. Intersections are roots of ϵ (marked by arrows). There are spurious intersections close to the branch cuts.

relative error. Furthermore, the integrals over J in the U_1 and U_3 regions are divided into two parts for treating separately the difficulties around $J = 4\sqrt{M_0}/\pi$ and $J = \infty$. For convenience, we also use the variable $k = \sqrt{(E(J) + M_0)/2M_0}$ instead of J to perform the integrations, where $E(J)$ is the energy associated with the action J.

Finally, we truncate the sum over $m \in \mathbb{Z}$ at ± 5. Going further did not change the results, up to our numerical precision.

E.3. Roots of $\epsilon(\omega)$

Due to the complicated structure of the dispersion function $\epsilon(\omega)$, we do not use any multidimensional root finding or minimization method. Rather, we chose to compute $|\epsilon(\omega)|$ on a large two-dimensional grid, to identify the regions where a root may exist; see figure E.1. After this preliminary computation, we plot the zero-level curves of $\mathrm{Re}(\epsilon(\omega))$ and $\mathrm{Im}(\epsilon(\omega))$. The roots of $\epsilon(\omega)$ are localized at the intersection points of these curves (see figure E.2). Let us stress that a careful analysis close to branch cuts is often needed.

Note added in proof. While we were in the final stage of preparation of this article, reference [46] was published, which provides criteria for the stability of inhomogeneous stationary states of the Vlasov equation, with the example of the HMF model. The method used in [46] yields simpler stability criteria than computing the roots of the dispersion relation. However, it provides less dynamical information than the method used in the present article.

References

[1] Neunzert H and Wick J, *Theoretische und numerische Ergebnisse zur nicht linearen Vlasov Gleichung*, 1972 *Numerische Lösung Nichtlinearer Partieller Differential und Integrodifferentialgleichungen* (*Lecture Notes in Math.* vol 267) (Berlin: Springer) pp 159–85 (Tagung, Math. Forschungsinst., Oberwolfach, 1971)

[2] Braun W and Hepp K, *The Vlasov dynamics and its fluctuations in the 1/N limit of interacting particles*, 1977 *Commun. Math. Phys.* **56** 101

[3] Campa A, Dauxois T and Ruffo S, *Statistical mechanics and dynamics of solvable models with long-range interactions*, 2009 *Phys. Rep.* **480** 57

[4] Chavanis P H, *Kinetic equations for systems with long-range interactions: a unified description*, 2010 *J. Stat. Mech.* P05019

[5] Balescu R, 1997 *Statistical Dynamics; Matter out of Equilibrium* (London: Imperial College Press) (Singapore: World Scientific)

[6] Chavanis P H, *Kinetic theory with angle–action variables*, 2006 *Physica* A **377** 469

[7] Manfredi G, *Long-time behavior of nonlinear Landau damping*, 1997 *Phys. Rev. Lett.* **79** 2815

[8] Barré J and Yamaguchi Y Y, *Small traveling clusters in attractive and repulsive Hamiltonian mean-field models*, 2009 *Phys. Rev.* E **79** 036208

[9] Landau L, *On the vibrations of the electronic plasma*, 1946 *J. Phys.—USSR* **10** 25

[10] Kalnajs A J, *Dynamics of flat galaxies. IV—the integral equation for normal modes in matrix form*, 1977 *Astrophys. J.* **212** 637

[11] Polyachenko V L and Shukhman I G, *General models of collisionless spherically symmetric stellar systems—a stability analysis*, 1981 *Sov. Astron. (Tr. Astron. Zh.)* **25** 533

[12] Palmer P L and Papaloizou J, *Instability in spherical stellar systems*, 1987 *Mon. Not. R. Astron. Soc.* **224** 1043

[13] Weinberg M D, *Self-gravitating response of a spherical galaxy to sinking satellites*, 1989 *Mon. Not. R. Astron. Soc.* **239** 549

[14] Weinberg M D, *Weakly damped modes in star clusters and galaxies*, 1994 *Astrophys. J.* **421** 481

[15] Bertin G, Pegoraro F, Rubini F and Vesperini E, *Linear stability of spherical collisionless stellar systems*, 1994 *Astrophys. J.* **434** 94

[16] Mathur S D, *Existence of oscillation modes in collisionless gravitating systems*, 1990 *Mon. Not. R. Astron. Soc.* **243** 529

[17] Weinberg M D, *Vertical oscillation of the Galactic disk*, 1991 *Astrophys. J.* **373** 391

[18] Louis P D, *Discrete oscillation modes and damped stationary density waves in one-dimensional collisionless systems*, 1992 *Mon. Not. R. Astron. Soc.* **258** 552

[19] Vesperini E and Weinberg M D, *Perturbations of spherical stellar systems during flyby encounters*, 2000 *Astrophys. J.* **534** 598

[20] Habib S, Kandrup H E and Yip P F, *Gravitational Landau damping for an isotropic cluster of stars*, 1986 *Astrophys. J.* **309** 176

[21] Briggs R J, Daugherty J D and Levy R H, *Role of Landau damping in crossed-field electron beams and inviscid shear flow*, 1970 *Phys. Fluids* **13** 421

[22] Corngold N R, *Linear response of the two-dimensional pure electron plasma: quasimodes for some model profiles*, 1995 *Phys. Plasmas* **2** 620

J. Stat. Mech. (2010) P08002

[23] Spencer R L and Rasband S N, *Damped diocotron quasi-modes of non-neutral plasmas and inviscid fluids*, 1997 *Phys. Plasmas* **4** 53
[24] Finn J M, del-Castillo-Negrete D and Barnes D C, *Compressional effects in nonneutral plasmas, a shallow water analogy and $m = 1$ instability*, 1999 *Phys. Plasmas* **6** 3744
[25] Schecter D A *et al*, *Inviscid damping of asymmetries on a two-dimensional vortex*, 2000 *Phys. Fluids* **12** 2397
[26] Pariev V I *et al*, *Stability analysis of hollow electron columns including compressional and thermal effects: integrability condition and numerical simulations*, 2002 *Phys. Plasmas* **9** 4863
[27] Pariev V I and Delzanno G L, *Stability analysis of hollow electron columns including compressional and thermal effects: initial value treatment*, 2003 *Phys. Plasmas* **10** 1262
[28] Kotelnikov I A, Pozzoli R and Romé M, *Diocotron instability in non-neutral plasmas with a stationary point in the rotation frequency profile*, 2005 *Phys. Plasmas* **12** 092105
[29] Volponi F and Okolicsanyi M, *Landau pole induced vorticity growth in a class of non-monotonic shear flows*, 2008 *J. Phys. A: Math. Theor.* **41** 145501
[30] Bouchet F and Morita H, *Large time behavior and asymptotic stability of the 2D Euler and linearized Euler equations*, 2010 *Physica* D **239** 948
[31] Inagaki S and Konishi T, *Dynamical stability of a simple model similar to self-gravitating systems*, 1993 *Publ. Astron. Soc. Japan* **45** 733
[32] Antoni M and Ruffo S, *Clustering and relaxation in Hamiltonian long-range dynamics*, 1995 *Phys. Rev.* E **52** 2361
[33] Inagaki S, *Kinetic equation for the modified Konishi–Kaneko system*, 1996 *Prog. Theor. Phys.* **96** 1307
[34] Inagaki S, *Thermodynamic stability of modified Konishi–Kaneko system*, 1993 *Prog. Theor. Phys.* **90** 577
[35] Caglioti E and Rousset F, *Long time estimates in the mean field limit*, 2008 *Arch. Ration. Mech. Anal.* **190** 517
[36] Jain K, Bouchet F and Mukamel D, *Relaxation times of unstable states in systems with long range interactions*, 2007 *J. Stat. Mech.* P11008
[37] Gluckstern R, *Analytic model for halo formation in high current ion linacs*, 1994 *Phys. Rev. Lett.* **73** 1247
[38] Benedetti C and Turchetti G, *Collective instabilities and collisional effects for space charge dominated beams*, 2007 *Nucl. Instrum. Methods Phys. Res.* A **577** 133
[39] Yamaguchi Y Y *et al*, *Stability criteria of the Vlasov equation and quasi stationary states of the HMF model*, 2004 *Physica* A **337** 36
[40] Abramowitz M and Stegun I A, 1964 *Handbook of Mathematical Functions* (New York: Dover)
[41] Weinberg M D, *Fluctuations in finite-N equilibrium stellar systems*, 1998 *Mon. Not. R. Astron. Soc.* **297** 101
[42] Bulirsch R, *Handbook series special functions, numerical calculations of elliptic integrals and elliptic functions*, 1965 *Numer. Math.* **7** 78
[43] Hofsommer D J and van de Riet R P, *On the numerical calculation of elliptic integrals of the first and second kind and the elliptic function of Jacobi*, 1963 *Numer. Math.* **5** 291
[44] Morita T and Horiguchi T, *Convergence of the arithmetic–geometric mean procedure for the complex variables and the calculation of the complete elliptic with complex modulus*, 1973 *Numer. Math.* **20** 425
[45] Morita T, *Calculation of the complete elliptic with complex modulus*, 1978 *Numer. Math.* **29** 233
[46] Campa A and Chavanis P H, *A dynamical stability criterion for inhomogeneous quasi-stationary states in long-range systems*, 2010 *J. Stat. Mech.* P06001

J. Stat. Mech. (2010) P08002